Numerical investigation of the heterogeneous combustion processes of solid fuels

Blaid Alganash, Manosh C. Paul[1] and Ian A. Watson

Systems, Power & Energy Research Division, School of Engineering, University of Glasgow, Glasgow G12 8QQ, UK

Abstract

Two-phase computational modelling based on the Euler-Euler was developed to investigate the heterogeneous combustion processes of biomass, in the solid carbon phase, inside a newly designed combustion chamber (Model 1). A transient simulation was carried out for a small amount of carbon powder situated in a cup which was located at the centre of the combustion chamber. A heat source was provided to initiate the combustion with the air supplied by three injection nozzles. The results show that the combustion is sustained in the chamber, as evidenced by the flame temperature. An axisymmetric combustion model (Model 2) based on the Euler-Lagrange approach was formulated to model the combustion of pulverized coal. Three cases with three different char oxidation models are presented. The predicted results have good agreement with the available experimental data and showed that the combustion inside the reactor was affected by the particulate size. A number of simulations were carried out to find the best values of parameters suitable for predicting NO_x pollutants.

Keywords: CFD; Multiphase flow; Heterogeneous combustion; pulverized combustion; NO_x formation

[1] Corresponding author: Manosh.Paul@glasgow.ac.uk, Tel: +44(0)141 330 8466

1. Introduction

There is a gradual transition globally to carbon-neutral fuels to potentially reduce global warming and at the same time, dependency on traditional carbon-based fuels such as coal, oil and natural gases which are facing the risk of depletion. The supply of energy has been dominated by fossil fuels for decades and currently, almost 80% of the world's energy is produced from fossil based fuels [1]. Coal and biomass are widely used for producing energy among the solid fuels and pulverized combustion is one of the common combustion technologies which utilise them.

While coal is causing serious environmental pollution and carbon dioxide emissions, it is still one of the important resources meeting the demand for power generation and about 45 % of the global energy demands was met by coal in the past decade [2]. On the other hand, biomass is environmental friendly and renewable for its carbon dioxide neutrality when it is utilised for energy production. Only about 10% of the world's current energy consumption is met by biomass [1], but this is considered to be one of the vital renewable sources of energy along with others such as wind, solar, hydro and geothermal. The interest, however, in using of biomass fuels for energy production across the world has been growing rapidly and it is potentially one of the options to replace fossil fuels causing emissions of greenhouse gases [3]. Particularly, the interest in using biomass within the European Union (EU) has strongly increased with a target to produce at least 20% of energy from renewable sources by 2020 [4].

Chemical compositions and molecular structures in any carbonaceous fuel, such as coal or biomass, are very complex. The main elements present in biomass, determined by ultimate analyses, are usually carbon (C), hydrogen (H), oxygen (O) and nitrogen (N). Other elements also found include sulphur, chloride and other impurities.

Despite the general similarities between the pulverised combustion of coal and that of biomass, there is a difference between their chemical compositions. Biomass has significantly lower fractions of carbon, while its oxygen content exceeds that of coal. The hydrogen fraction is also somewhat higher than that of coal. The typical weight percentages for C, H and O, respectively are 30 to 60 %, 5 to 6 % and 30 to 45 % [1]. For coal, the typical compositions (mass percentages) include 65 to 95% C, 2 to 7% H, up to 25% O and 1 to 2% N [5]. Moreover, there is also a difference between biomass and coal regarding their

devolatilization. Compared to coal, biomass has a much higher amount of volatile matter leading to a dominating role of devolatilization in the overall conversion process of biomass particles. The volatiles fraction in biomass is usually 70-80%, whereas the fraction in coal is 10-50%. The high level of volatiles makes biomass a combustible fuel which means that it is easier to ignite even at low temperature. However, it has lower energy content due to the higher O/C and H/C atomic ratios when compared to coal. With anthracite less than 10% and bituminous from 5 to 6%, biomass fuels can lose up to 90% of their masses during the process of devolatilization [1]. The devolatilization of biomass and coal has been extensively investigated in [6-9]

In numerical simulations, most researchers for simplicity considered the combustion of solid fuels occurring in two individual steps. The first one is the combustion of volatiles and the second one is the combustion of char, neglecting the interaction between the two steps. But, for any two-phase flow, such as pulverized coal combustion, the interactions between the gaseous and solid phases needs to be taken into account because such a type of flow is characterized by non-linear coupling between the two phases such as gas turbulence influencing both the particle motion and heat up. This requires an accurate description of both the continues gas phase and the dispersed particle phase. This may be studied by using the Euler-Lagrange or Euler-Euler modelling approaches and it is crucial for practical application of prediction of solid fuels combustion for different technologies.

Pulverized combustion is characterized by small volume fraction of the dispersed particle phase and as a result, in this study, the former approach was used to model the pulverized coal combustion in Model 2, whereas the later one was applied in Model 1.

Several models adopted Lagrangian approach in treating the particle phase when modelling pulverized coal combustion [10-12]. Concerning the biomass combustion, the Lagrangian approach was used by Fletcher [13] to simulate the flow and reactions inside an entrained biomass gasifier and the numerical results showed the capability of the Lagrangian model to optimise the design of such gasifiers. Another study regarding the modelling of pulverized wood combustion was carried out in which the Lagrangian manner was also adopted [14]. Additionally, several recent studies successfully used the Euler-Euler approach in modelling wood gasification in a fluidised bed reactor [15], dispersed two-phase flow in pulverized coal combustion [16] and coal gasification in a fluidized bed reactor [17] .

Furthermore, combustion of solid fuels such as coal and biomass influences the environment mainly through emissions of nitrogen oxides (NO_x) to atmosphere. These emissions are associated with a variety of environmental concerns such as the formation of acid rain and photochemical smog in urban air. In a combustion system, including pulverized combustion, the formation and destruction of NO_x emissions are influenced by several factors such as fuel properties and, combustion conditions e.g. temperature of reaction and the fuel-air ratio [18]. Nitrogen from combustion of solid fuels with air is then converted to pollutants: nitric oxide (NO), nitrogen dioxide (NO_2), nitrous oxide (N_2O), ammonia (NH_3) and hydrocyanide (HCN). NO_x oxides include mostly NO and much lower concentration of NO_2 and N_2O. So, NO_x modelling is particularly focussed on the prediction of NO concentration in the reactive field of interest. However, in combustion systems of solid fuels without considering the nitrogen contained in fuels (fuel-N), NO_x emissions formed at high temperatures from nitrogen of the combustion air, can be limited by combustion engineering measures to allowable values. On the other hand, when using nitrogenous fuels and low combustion temperatures, the formation of NO_x is mainly due to the conversion of fuel-N, partially or totally into nitrogen oxides [19].

The overall aim of this study is to provide a deeper understanding on the process of heterogeneous combustion of solid fuels by applying computational fluid dynamics techniques. In particular, the objectives include the following:

- To study the interactions between the gas and solid phases of fuels during the combustion process.
- To develop a combustion model that takes into account the different gas-solid behaviours, heat transfer and thermal conversion processes, by using multiphase modelling.
- To investigate the formation of nitric oxide (NO) during combustion.

2. Combustion mechanisms and heterogeneous reactions

Four well-defined steps are usually involved in the chemical processes of solid fuel combustion: drying, devolatilization, volatile combustion and char oxidation. Once solid fuels are injected into a combustion chamber, they are heated up and the drying process (the release of moisture) occurs immediately, followed by the rapid devolatilization process (the release of volatiles) which occurs due to high temperatures. Char produced through the

volatilization process is consumed by heterogeneous processes of combustion and gasification and its combustion yields carbon monoxide (CO) and carbon dioxide (CO_2) according to the following reactions:

$$C(s) + O_2 \rightarrow CO_2 \quad \textbf{(R1)}$$

$$C(s) + 0.5O_2 \rightarrow CO \quad \textbf{(R2)}$$

$$C(s) + CO_2 \rightarrow 2CO \quad \textbf{(R3)}$$

Reactions (R1) and (R2) are exothermic and will occur very rapidly but reaction (R3) is endothermic. In general, a dominating heterogeneous reaction is related to whether the char combustion rate is limited by either the diffusion of oxygen through the boundary layer surrounding particles or the kinetic rate of carbon oxidation reactions. Heterogeneous reactions can also include the following endothermic reaction:

$$C(s) + H_2O \rightarrow CO + H_2 \quad \textbf{(R4)}$$

where the carbon monoxide (CO) and hydrogen (H_2) resulting from reactions (R3), (R4) and (R5) are incorporated to the gas phase and oxidized to CO_2 and H_2O according to the following homogeneous reactions:

$$CO + 0.5O_2 \rightarrow CO_2 \quad \textbf{(R5)}$$

$$H_2 + 0.5O_2 \rightarrow H_2O \quad \textbf{(R6)}$$

However, for the Eulerian-Eulerian simulation (Model 1), the only reaction included is (R1). The combustion rate of char is assumed to be limited by the chemical kinetics because the only reactive species that is included in the gas phase is O_2. Then, the reaction rate r_a (kmol/m^{3}s) is defined as

$$r_a = k_a . C_{c(s)} . C_{o_2} \quad (1)$$

where $C_{c(s)}$ and C_{o_2} (kmol/m^3) are the concentrations of carbon and oxygen respectively; and k_a is the reaction rate constant given by the Arrhenius type relation:

$$k_a = AT^{\beta} \exp(-\frac{E}{RT}) \quad (2)$$

where A, β, E, R and T are the pre-exponential factor, temperature exponent activation energy, universal gas constant, and temperature, respectively.

For the Eulerian-Lagrangian simulation (Model 2), the pulverized coal combustion model proposed in this simulation involves devolatilization, volatile combustion, char combustion and other gas phase reactions. In this study, volatiles release is described by the single rate model. It assumes that the rate of devolatilization is first-order dependent on the amount of volatiles remaining in the particle and employs global kinetics. The reaction and its rate constant are:

$$coal \xrightarrow{k_d} volatile\ (\alpha) + \ char\ (1-\alpha) \quad \textbf{(R7)}$$

where α is the distribution coefficient.

$$k_d = A \exp(-E/RT) \quad (3)$$

The heterogeneous reaction begins after the volatile fraction of coal particles is completely evolved. The initial reaction considered in this simulation is the oxidation of combustible fraction of coal particle (char) to carbon dioxide. The models that are applied to calculate the reaction rate are the diffusion model [20] for case 1, and the kinetics/diffusion model [21] rate models for case 2. It assumes that the heterogeneous reaction rate is determined by the diffusion of the gaseous oxidant to the surface of the particle in the former model, and is determined either by the diffusion rate or by a chemical reaction, presumed to be first order in oxidant partial pressure and occurring entirely at the particle surface, in the latter one. With regard to case 3, the multiple surface reaction model was used. According to this model, the rate of particle species depletion for any reaction is given by

$$\bar{r}_{het} = A_p\, \eta\, Y_i\, R_{i,r} \quad (4)$$

where A_p, η, Y_i and $R_{i,r}$ are the particle surface area (m^2), effectiveness factor, mass fraction of surface species *i* in the particle and rate of particle species depletion (kg/sec).

$$R_{i,r} = \mathcal{R}\left(P_n - \frac{R_{i,r}}{D_o}\right)^N \quad (5)$$

where P_n, D_o, $\mathcal{R}$ and N are bulk partial pressure of the gas phase species (pa), the diffusion and kinetic rate and apparent order of reaction, respectively.

$$D_o = C_1 \frac{\left[(T_p + T_g)/2\right]^{0.75}}{d_p} \quad (6)$$

where C_1 is the mass diffusion limited rate constant (C_1 = 5x10^{-12} m^3/K$^{0.75}$s).

$$\mathcal{R} = AT^{\beta} e^{-(E/RT)} \quad (7)$$

Then, the rate of particle surface species depletion for a reaction with order (N = 1) is given by

$$\bar{r}_{het} = A_p\, \eta\, Y_i\, P_n \frac{\mathcal{R} D_o}{\mathcal{R} + D_o} \quad (8)$$

and for a reaction with order (N=0),

$$\bar{r}_{het} = A_p\, \eta\, Y_i \mathcal{R} \quad (9)$$

In the gas phase reactions, the yields of gases and tars combined are known as the volatile matter (hv_vol) which will evolve during the devolatilization process. This volatile matter, for simplicity in this study and also because the detailed chemical species in it are not completely understood due to the complexity of the chemical structure of coal, was generally treated as a single species which varies depending on the type of coal and comprising carbon, hydrogen and oxygen (CH_xO_y) in a ratio determined from the ultimate analysis of coal according to the following homogeneous reaction:

$$CH_xO_y + aO_2 \rightarrow CO_2 + bH_2O \quad \textbf{(R8)}$$

where x and y represent the composition of the chemical elements.

Thus, equating the numbers of atoms of each element in the reactants to the number in the products gives:

$$a = (1 + x/4 - y/2) \quad (10)$$

$$b = x/2 \tag{11}$$

For the coal used in this study, the volatile gas species are represented in the CFD predictions as $CH_{3.392}O_{0.33}$ which was calculated from the coal's ultimate and approximate analysis. It provides the stoichiometric coefficient of (a =1.683). The finite rate / eddy-dissipation model that calculates both the Arrhenius kinetic and eddy-dissipation [22] rates was applied in the simulations to account for the turbulence chemistry interaction and the net reaction rate is chosen as the minimum of the two rates depending on which one is dominating the local reactions.

$$r_i = min(r_{Arr}, r_{Edd}) \tag{12}$$

The Arrhenius kinetic and eddy-dissipation rates are, respectively, given as

$$r_{Arr} = AT^{\beta}\, exp\left(-\frac{E}{RT}\right)[C_R]^d[C_{ox}]^e \tag{13}$$

where C_R and C_{ox} are reactant and oxidant concentrations, respectively.

$$r_{Edd} = 4\nu'_{i,r}M_{w,i}\rho\frac{\varepsilon}{k}\min\left[\min_R\left(\frac{Y_R}{\nu'_{R,r}M_{w,R}}\right), \frac{\sum_{\mathcal{P}} Y_{\mathcal{P}}}{2\sum_j^N \nu''_{j,r}M_{w,j}}\right] \tag{14}$$

where $M_{w,i}$ is the molecular weight of species i, $Y_{\mathcal{P}}$ is the mass fraction of any product species, Y_R is the mass fraction of a particular reactant R, N is the number of species, $\nu'_{i,r}$ is the stoichiometric coefficient for reactant i, and $\nu''_{j,r}$ is the product species stoichiometric coefficient and it will be zero for any species that is not a product in the reaction.

Six chemical reactions are considered: the heterogeneous ones (R1) through (R4) and the gaseous reactions (R5) and (R8). A summary of the kinetics data used in the present combustion modelling and the values of *d* and *e* are provided in Table 1 [23-26].

2.1 Chemistry of pulverised coal

Simulations of the pulverised coal combustion have been carried out on bituminous coal. The proximate and ultimate analyses are shown in Table 2. It appears that the low heating value is higher than that of pure carbon (around 33 MJ/kg) because the high heating value was estimated on the dry ash free (DAF) using the correlation given in [27].The formulation of the coal used in the numerical modelling has been simplified in a form that makes the numerical simulations simpler. For example, the content of Sulphur (S) and Nitrogen (N) has been eliminated from the ultimate analysis. The dry ash free (DAF) composition of coal is 86.32% C, 5.36% H and 8.32% O. The elemental composition and the enthalpy formation of volatile are determined from the proximate and ultimate analysis data of the coal. The standard enthalpy of formation of the volatile was -5.8247034 $*10^7$ J/kmol. The volatile has the simplified molecular formula $CH_{3.392}O_{0.33}$ and a molecular weight of 20.672 kg/kmol.

2.2 NO_x model

Different mechanisms during the combustion of solid fuels cause the formation of NO_x e.g. thermal-NO, prompt-NO and fuel-NO . However, in a solid fuel combustion system, the oxidation of fuel-NO is typically the most significant source of production of NO_x during the combustion process with some contribution from the thermal-NO. It has been shown in [28] that over 80% of the NO formed in pulverised coal combustion derives from the coal i.e. they result from the oxidation of nitrogen in the coal (coal-N), and the remainder is due to the thermal and prompt NO. In addition, the experimental research carried out by Pershing and Wendt [29] demonstrated that the contribution of thermal NO becomes significant when the temperatures in the coal flames are greater than 1650 K.

In this work, thermal-NO and fuel-NO were considered. For the former one, NO was predicted by using the extended Zeldovich mechanism with the partial equilibrium approach for radicals O and OH concentrations. The only two mechanisms considered in this study are the thermal-NO and the fuel-NO. For the former one, NO is predicted by using the extended Zeldovich mechanism with the partial equilibrium approach for radicals O and OH concentrations. With regard to the fuel-NO mechanism, most coals contain 0.5-2.0% nitrogen by weight, bituminous coals generally have high nitrogen levels and anthracite low nitrogen levels. It was assumed that the nitrogen contained in the coal is completely devolatilised

during the simulations and distributed between the volatiles and the char when a coal particle is heated. This distribution is indicated by most experimental studies of coal pyrolysis [30]. The split of nitrogen in the fuel into volatiles and char is important for NOx formation. Consequently, nitrogen release from both the coal pyrolysis and char oxidation must be considered when modelling NOx reactions in coal combustion systems. The key issue is the knowledge of partitioning of the nitrogen between them. The fraction of nitrogen released with the volatiles depends on the fuel type, temperature, and residence time [31]. The increase in temperature and residence time favours the conversion of coal-N to volatile-N.

In some studies [32], it was assumed that the fuel nitrogen is distributed evenly between the volatiles and the char. Accordingly, a parameter γ (char nitrogen as a fraction of total coal nitrogen) is introduced to describe this distribution as follows:

$$m_{vol}^{N} = (1-\gamma) * \frac{m_{tot}^{N}}{F_{vol}} \quad (15)$$

$$m_{char}^{N} = \gamma * \frac{m_{tot}^{N}}{F_{char}} \quad (16)$$

where $\gamma \in \langle 0,1 \rangle$; m_{vol}^{N}, m_{char}^{N}, m_{tot}^{N}, F_{vol} and F_{char} are the mass fractions, of nitrogen in volatiles, the mass fraction of nitrogen in char, the total mass fraction of nitrogen in DAF coal, the mass fraction of volatiles in DAF coal and mass fraction of char in DAF coal, respectively.

The transformation of nitrogen to pollutants takes place via intermediates HCN and NH_3.
The reactions considered for NO formation and the reactions that lead to the reduction of NO are as follows:

$$HCN + O_2 \xrightarrow{R_1} NO + \cdots \quad \textbf{(R9)}$$

$$NH_3 + O_2 \xrightarrow{R_2} NO + \cdots \quad \textbf{(R10)}$$

$$HCN + NO \xrightarrow{R_3} N_2 + \cdots \quad \textbf{(R11)}$$

$$NH_3 + NO \xrightarrow{R_4} N_2 + \cdots \quad \textbf{(R12)}$$

The rate of conversion of HCN and NH_3 are given by De Soete as

$$R_1 = A_1 X_{HCN} X_{O_2}^a exp(-E_1/RT) \quad (17)$$

$$R_2 = A_2 X_{HN_3} X_{O_2}^a exp(-E_2/RT) \quad (18)$$

$$R_3 = A_3 X_{HCN} X_{NO} exp(-E_3/RT) \quad (19)$$

$$R_4 = A_4 X_{HN_3} X_{NO} exp(-E_4/RT) \quad (20)$$

where X is the mole fraction, a is the oxygen reaction order and T is the instantaneous temperature (K). The kinetics of these reactions are given in Table 3 and the oxygen reaction order is taken from Table 4.

Regarding the NO reduction on char surface, the heterogeneous reaction by which the reduction of NO occurs on the char surface is given as

$$C(s) + NO \overset{R_5}{\rightarrow} N_2 + \cdots \quad \textbf{(R13)}$$

The reaction rate (R_5) is defined as

$$R_5 = A_5 \exp(-E_5/RT)\, A_E P_{NO} \quad (21)$$

where P_{NO} is the NO partial pressure calculated by using the Dalton's law: $P_{NO} = X_{NO} P$, T is the mean temperature (K) and A_E is the external surface area of the char in (m^2/kg). The kinetic constants of this reaction are $A_5 = 2.27\text{x}10^{-3}$ (mol/pa/s/m^2_{BET}) and E_5 = 142737.485 J/mol.

3. Overview of the numerical procedures

Reynolds-averaged Navier-Stokes (RANS) equations comprising the conservation of mass, momentum, energy and concentration of species are solved with a standard two-equation k-ε turbulence model for the gas phase. Such equations are Eulerian ones and solved for the velocity, pressure, temperature, species mass fractions, turbulence kinetic energy and turbulence dissipation energy at every point of the computational domain. However, in the Lagrangian approach, the trajectory of discrete phase particles is determined by solving its equations of motion in the particle phase. The P-1 radiation model is employed for the heat transfer of radiation with a cell based WSGGM (weighted-sum-of gray-gases model) to calculate the absorption coefficient of the gas phase.

FLUENT uses an implicit finite volume method to discretise the conservation equations with a pressure-velocity coupling derived by the SIMPLE (Semi-Implicit Method for Pressure linked equations) algorithm [33]. The discretisation process is done via a second order upwind scheme and the evaluation of gradients and derivatives is carried out by a Green-Gauss cell based Gradient Evaluation method. For getting a stable solution, the relaxation factors have been adjusted and the residual for all the variables converged to 10^{-4} but for the energy and radiation to 10^{-6}. Boundary conditions as well as relevant operating conditions used in the numerical simulations are described in the results sections below.

Due to the reason that the concentration of NO formed is so small compared with the concentration of other species of interest in the combustion process, the reactions included in the NO chemistry have been decoupled from the pulverized coal combustion process, i.e. the models of nitrogen pollutants are decoupled from the combustion model and executed after the flame structure has been predicted. Thus, the method used for NOx modelling in RANS simulations and particularly in Fluent is the one by which the chemical formation and reduction rates of NO are calculated by post-processing data obtained from a previously reacting flow simulations. Another advantage of this method is the computational efficiency. Standard Fluent NO-post-processing models considering thermal-NO and fuel-NO formation were used and the species transport equations for the mass fraction of NO, HCN, and NH_3 were solved.

Moreover, during the process of pulverized combustion, devolatilization takes place rapidly, followed by the oxidation of the devolatilized products (volatiles) such as tar and light gases. When these volatiles are released much of the nitrogen content in the coal particles is also released. However, the nitrogen contained in the fuel is partially released in both the volatiles and the char. The split of nitrogen in the fuel into volatile-N and char-N is potentially important for the NO_x formation. It is assumed that the fuel nitrogen is distributed between the volatiles and char according to the parameter γ which takes the value of 0.2. This assumption has been made because the conversion of the nitrogen released in the volatiles to NO_x is predominant during the pyrolysis in pulverized fuel flames. Furthermore, as already mentioned in § 2.2 the nitrogen is depleted at high temperatures but at low temperatures it is retained in the char. In particular, at higher temperatures (above 1500K), up to 70-90% of coal nitrogen is devolatilized [34] and pulverized fuel furnaces produce high temperature which results in releasing most of the coal nitrogen with the volatiles. In regular pulverized

coal combustion, about 60-80% of NOx results from the volatile-N [35]. Thus, by using the value $\gamma = 0.2$ the mass fractions of nitrogen in both the volatiles and char are calculated using equations (15) and (16).

Yang et al. [36] showed that the volatile matter for the bituminous coals is most important for the NO_x-forming property, and the volatile-N consists mostly of tarry compounds that decay rapidly to HCN at high temperatures. In addition, the combustion of the bituminous coals show more HCN formation than NH_3 [37], thus leading to the assumption that the nitrogen is released via the intermediates HCN and NH3 with a higher percentage of the former one. The percentages used for different simulation runs of the two species are shown in Table 5 and, depending on the local conditions, these two species react to form either NO or N_2. For the char nitrogen pathway however, it is assumed that all the nitrogen is released via the intermediate HCN [38].

4. Results of Combustion Model 1

The geometry of a newly designed combustion chamber is shown in Figure 1(a) which consists of a small cup located in the centre of the chamber. The chamber was designed to enable experimental work to provide data for validating the theoretical data. The computational domain is a cylinder with an internal diameter of 48 mm and length of 101 mm. The dimensions of the cup are 20 mm in diameter and 10 mm in height. Solid carbon particles are placed in the cup and for the dispersion of the particles, the air is supplied through the three injection nozzles, each having a diameter of 3 mm, as shown in Figure 1(b). The nozzle in the middle was made with an angle of 30° from the horizontal line for the sake of injecting the air into the centre of the cup. The geometry of the combustion chamber was created by using solid works which was then exported to the pre-processor GAMBIT to generate the mesh and specify the boundary conditions, as shown in Figure 1(b, c).

For the boundary conditions, the velocity-inlet was selected with an air inlet velocity of 1m/s. The pressure outlet (i.e. the zero gauge pressure) was selected at the outlet of the chamber as shown in Figure 1(b) and the walls are stationary with no-slip condition. The combustion simulations are performed for particle sizes with different average diameters (0.5, 1, 1.5, 2, 2.5 and 3). An unsteady-state solver with a time-step of 10^{-3} s was used.

The combustion modelling is based on the two-phase Euler-Euler approach which takes into account the interactions of the gaseous and solid phases. The char combustion is considered by the single-step heterogeneous reaction (R1). A user-defined function (UDF), with which the rate of the heterogeneous chemical reaction between the solid and gas phases is defined, developed and coded in C++ language and incorporated in the solver. Some assumptions are made to simply the combustion modelling: the solid carbon particles are assumed to be inelastic and mono-dispersed spheres which represent a pure (100%) carbon. In reality, this is not the case and to some extent the existence of inherent moisture, sulphur, nitrogen, and other non-carbon components will affect combustion characteristics as described in §2. Moreover, the virtual mass effect is neglected because the density of the solid phase is greater than that of the gas phase. Since the particle size is small the lift force, due to the velocity gradients in the gas-phase flow field, is not significant and as a result it has also been neglected. Therefore, the interaction between the phases is only due to the drag force.

Initially, a grid-refinement test is carried out in order to estimate the grid size and mesh quality required for the simulation. It is commonly known that more accurate solutions can be obtained from numerical simulations with a higher number of computational mesh cells. Therefore, a grid-refinement test is carried out for the coal particle size of 1 mm by sequentially increasing the number of control volumes inside the chamber. The peak combustion temperature presented in Figure 2 against time (sec) shows that the variation in the results obtained by the two relatively higher resolution grids (551486 and 977899) is very moderate. And the results obtained by the grid cell size of 474748 lay between the results of the highest and lowest density grids. Thus, one of these relatively higher resolution grids will be suitable for the simulations, but in order to save the computational time the grid size of 474748 is used to perform all the numerical simulations in Model 1.

For the case of a 1mm average particle diameter, the volume fraction at different simulation time-steps is shown in Figure 3. At the beginning the volume fraction was set to 0.6, and the results taken in the mid-plane of the combustion chamber show that the volume fraction of the solid phase progresses upward through the chamber. It can also be seen that the carbon particles move upward where a good mixing of the particles and the injected air through the nozzles was obtained.

Particularly, the results show that some particles accumulated at the centre of the top wall of the chamber after 0.2 sec and this can be identified by referring to Figure 4, which illustrates

the high temperature zone inside the chamber at the different time-steps. From the temperature distribution in Figure 4, it is also clear that the combustion was sustained and the temperature of the gas phase rapidly propagates upward from the cup due to the release of heat during the process of combustion. Moreover, the temperature contour profiles further show that the location of the combustion zone moves to the top section of the chamber with time, and the waviness seen in the contours in the lower right region is attributed to the air injection from the three nozzles.

The concentration of carbon dioxide (CO_2) is depicted in Figure 5. It can be seen that the concentration of CO_2 is also changing with the time. The concentration at the time of 0.2 sec also indicates the accumulation of the carbon particles at the centre of the top wall of the chamber as mentioned above.

Figure 6 shows the variation of the peak temperature inside the chamber with time for cases with different particle diameters. At the beginning the temperature was 1200 K and when the combustion took place it increased with time. It is clear that the size of particle plays a crucial role in the combustion process as can be seen from this figure. As the particle size decreased, the peak temperature of the gas phase decreased. The larger the particle size the higher the peak temperature. It is shown that the highest temperature was obtained from the case of carbon particles with an average diameter of 3 mm and the lowest temperature was gained by burning carbon particles with an average diameter of 0.5 mm. It is also shown that the peak temperatures of the gas phase is getting close to each other for short times, ~ 0.6 sec, then the temperature of the smaller particles size increases when compared with that of the larger particles. This may be attributed to the accumulation of the smaller particles at the top of the chamber, as can be seen from Figure 3 and Figure 4, for the case of 1 mm average particle diameter. This is further related to the design of the combustion chamber which means that the height of the chamber needs to be increased to accommodate more space for the dispersion of particles so they can mix well with the air. Furthermore, combustion is enhanced by increasing the fuel surface area exposed to the oxidizer, which is the air by reducing the size of the particles. In this case and due to the accumulation of fuel particles at the top of the chamber, the particles with smaller sizes accumulated with greater concentration than that of the larger ones. This may result in the smaller particles producing higher temperature than the larger ones.

5. Results of Combustion Model 2

The basic geometry of the reactor considered for this study is taken from Zhang et al. [39]. The reactor is 2.5m in length with an internal diameter of 200 mm. An axisymmetric computational domain and the burner of the reactor that consists of three concentric tubes are shown in Figure 7. The coal particles are injected centrally through an 8 mm diameter inner tube. A concentric tube with a diameter of 18mm makes an annular gap that admits the primary air through it. The secondary air is supplied through another annular gap made by a concentric tube with a diameter of 34mm. The operating conditions are shown in Table 6. Some assumptions are made in order to simplify the modelling e.g. it is assumed that the gas phase can be treated as an ideal-gas mixture and the coal particles are assumed to be spherical in shape and enter the combustor at the same velocity as the carrying air. The initial temperature of coal particles is 300K and the side walls are modelled as having a constant temperature maintained by an electrical heater. The interaction between the particles in this case is neglected.

The model used in the simulation is the discrete phase Eulerian-Lagrangian model. Three cases were simulated. In the first two cases, the char was assumed to be only oxidized to CO_2 according to the reaction (R1). The char oxidation in the first case (Case 1) was simulated by the diffusion model while the diffusion-kinetics model was used in the second case (Case 2). In the third case (Case 3), the combustion of char was assumed to follow the reactions (R1) through (R4). To determine the rates of these reactions, UDFs were written and exported to the solver, and the other processes were modelled using sub-models which are readily available in FLUENT such as turbulence, turbulence-chemistry interaction, radiation, particles initial heating up, particles devolatilization, NO_x models, etc. Furthermore, the particle size distribution of the pulverized coal particles injected into the reactor is assumed to follow a Rosin-Rammler distribution curve based on the assumption that an exponential relationship exists between the particle diameter (d_p) and the mass fraction of particles (Y_d) with diameter greater than d_p:

$$Y_d = e^{-(d_p/\bar{d})^n} \quad (22)$$

where $\bar{d}$ is the mean diameter and *n* is the spread parameter. The stochastic tracking (random walk) model [40] was used to predict the dispersion of the particles due to the turbulent motion of the gas-phase. Six discrete particles have been considered to describe a single

particle size in order to get a realistic representation of the average particle trajectories. One way coupling has been assumed. The dispersion of the particles due to turbulence in the gas phase is predicted by using a stochastic tracking model.

A steady state computation was initially carried out with a grid resolution having a total of 48000 control volumes. The grid density was slightly reduced to 37500, and then symmetrically increased to 52000, 61000 control volumes to check their sensitivity on simulated results. Figure 8 shows the temperature inside the reactor along the mid-line for the four grids and the predicted results show reasonably good agreement with small variation at the upstream of the reactor. In order to validate the model, the simulation results are compared with the experimental data [39] and shown in Figure 9. It can be seen that the predictions of O_2 and CO_2 concentrations generally have a good agreement with the experimental data. In particular, the mass fraction of oxygen along the axial distance of the reactor in Figure 9(a) shows the results predicted by Case 3 are closer to the experimental results near the burner than the other two cases, while Case 1 results show better agreement at the exit of the reactor. The mole fractions of carbon dioxide in Figure 9(b) also show that the Case 3 results have very good agreement with the experimental data. We note that Zhang et al. [39] also performed CFD investigations in the same combustion chamber, and the results predicted by the current simulation approaches are far better than their results. They used an Eulerian-Eulerian model while the current simulations results proved that the discrete phase Eulerian-Lagrangian model is a best suited method for this particular application of modelling coal combustion.

In order to further estimate quantitatively the difference between the experimental and numerically predicted results, a parity plot of the O_2 mass fraction and CO_2 mole fraction at the different axial locations are presented in Figure 10. The $y = z$ line indicates the ideal results i.e. the simulated results are identical to those from the experiment. From Figure 10(a) for the oxygen mass fraction, it can be seen that the results of Case 3 has very good agreement as most of the data points lie very close the line when compared with the other cases. Results of Cases 1 and 2 have good agreement with the experiment towards the downstream of the reactor but failed to achieve better accuracy near the burner region as can be seen at the axial distances $x \approx 0.142$ m and $x \approx 0.2$ m where the data placed far from the line. The same is seen in Figure 10(b) for the carbon dioxide mole fraction. However, we further emphasise that no information is available in Zhang et al. [39] on the standard

deviation of these experimental data and in practise this has to be taken into account in any comparative plot, and overall, as already mentioned, Case 3 produces the best agreed results.

The volatile mass fraction is illustrated in Figure 11(a). It is seen that the behaviour of the volatile release is almost the same in general for all the cases but the start of volatile release shifts to a downstream location of the reactor for Cases 1 and 2. The variation of gas temperature inside the reactor for all the cases is depicted in Figure 11(b). It is found that the higher temperatures are located in the region where the volatile combustion occurs, which can be identified by the release of volatiles as shown in Figure 11(a).

Figure 12 gives a clear view of the temperature distribution of the gas phase. Again, the maximum temperature occurs where the volatile releases and the oxidation happens. It is shown that the temperature distributions are the same near the exit of the reactor. The variation of temperature inside the reactor indicates the process of the coal combustion when referring to Figure 11(b). Once the particles of coal mix with the air at the feed point, the mixture temperature initially drops due to the heat taken by the coal particles for devolatilization. Then the temperature rises gradually, followed by a sudden increase as a result of the combustion of volatiles and char.

Figure 13(a) depicts the mass change of coal particles along the axial distance of the reactor. It is seen that there is a flat part of the curves at the beginning for each particle, which means that there is no mass change taking place and the particles only undergo a heating process. It can also be seen that the larger particles need a longer period of time to be heated up than that of the smaller particles. Then, there is a decrease in the mass due to the particles devolatilization which takes place rapidly for the small particles and is slower for the larger particles. During the devolatilization the volatile matter is released.

Figure 13(a) also shows that for particle size the whole volatile matter was almost released and the char reactions began. From the properties of the coal, the solid combustible fraction of DAF coal was approximately 67%, and it is found that the decrease in mass reaches this value, which means that nearly the total volatile matter was released. This reduction in mass is accompanied by the volatile combustion and this can be identified when referring to Figure 11(b), where it was found that the highest rate of change of temperature occurred in the region between 0.1m and 0.4m due to the rapid change of mass of the small particles. This effect is now clearly examined from Figure 13(a), where the results show that the particles

with smaller diameters (e.g. 16 and 84 μm) rapidly lost their mass, at a faster rate than the larger particles. For the larger particles, the heat release by combustion is taken up by the endothermic reactions, causing a slower decrease in their mass. Furthermore, when the heat is released by combustion and the oxygen is almost depleted, the gas temperature decreases gradually.

Figure 13(b) shows the burnout percentage of the particles, which is a measure of the extent of the combustion of coal particles. It can be seen that the particle size has a great effect on the coal burnout. The burnout of particle with a diameter of 16 μm is 100%. Whereas, the burnout of particles with diameter of 84, 154, 222 and 291 μm at the exit of the combustion domain is approximately 86, 75, 35, 33 and 29 %, respectively. This leads to the conclusion that when the particle size increases the burnout decreases.

Figure 14 shows the calculated NO emissions for the third case of pulverized combustion modelling (Case 3) for different runs. It shows the effect of the intermediates on the formation of NO. All the runs gave the same trend, but it is clear that the run with the assumptions: 52% HCN, 10% NH_3 and 38% NO has very good agreement with the experiment data available in [41]. Further, it can be seen that the calculated profile of NO concentration is rather smooth except at the upstream where there is a slight difference found between the measured and calculated values. On the other hand, it gives very good agreement in the downstream towards the exit of the reactor. Referring to Figure 14, it is seen that the variation of intermediate percentages has an influence on the formation of NO. Thus, the decrease of the assumed HCN percentage results in increasing the mass fraction of NO.

6. Conclusion

Heterogeneous combustion process of coal in the first combustion chamber (Model 1) has been simulated using the Euler-Euler numerical method. Simplification to the heterogeneous reaction of coal was made and the chemical reaction rate was defined in ANSYS FLUENT 6.3.26 software by incorporating a user defined function (UDF). The results presented show that the combustion was sustained in the chamber, as evidenced by the flame temperature distribution. The temperature was affected by the size of the coal particles. The second model (Model 2) has been formulated to predict the combustion of pulverized coal. The results show good agreement with the experimental data. They also showed that the combustion inside the reactor was affected by the particles size. In comparison with the

larger particles, it was shown that the volatiles from smaller particles released rapidly and the gas temperature reached its maximum, followed by a decrease due to the start of the endothermic reactions. Moreover, increasing the diameter of the coal particles reduces the coal burnout at the exit of the reactor.

In terms of the thermal Biot number, which relates the internal heat transfer resistance to the external resistance, the discrete phase model used in the combustion simulation for the different particle sizes is based on the thermally-thin assumption that considers a uniform temperature distribution throughout the particles. However, Yang et al. [42] showed that a much advanced numerical method "doublemesh scheme" is suitable for a thermally-thick combustion process for a biomass fuel with sizes ranging from 10 mm to 100 mm usually used in packed-bed combustion systems. In those applications, the temperature gradients will exist within the particles and affect the evaporation as well as devolatilization rates during the combustion process.

The NO_x concentration at the furnace exit (Model 2) was calculated and the results of Run 3 gave the best combination of parameters when compared with the experimental data.

References

[1] A. A. Khan, W. D. Jung, P. J. Janssen, and H. Spliethoff, “Biomass combustion in fluidized bed boilers : Potentials, problems and remedies”. Fuel Processing Technology. 2009, 90: pp.21-50.

[2] “ Energy outlook 2012”, International Energy Agency, 2012.

[3] J. Tissari, O. Sippula, J. Kouki, K. Vuorio, and J. Jokiniemi., “Fine particle and gas emissions from the combustion of agricultural fuels fired in a 20 kW burner”. Energy & Fuels. 2008, 22: pp.2033-2044.

[4] M. Hoogwijk, A. Faaij, B. Eickhout, and W. Turkenburg, “Potential of biomass energy out to 2100 for four IPCC SRES land-use scenarios”. Biomass and Bioenergy. 2005, 29: pp.225-257.

[5] R. H. Essenhigh, “Combustion and flame propagation in coal systems”. In: Sixteenth Symposium (International on combustion, Combustion Institute, Pittsburgh, 1977, pp.353-374.

[6] R. S. Parikh, and R. Mahalingam, “Modeling and experimental studies on devolatilization yields from a bituminous coal”. Ind. Eng. Chem. Res. 1987, 26: pp.2378-2384.

[7] Y. A. Levendis, K. Joshi, R. Khatami, and A. F. Sarofim, “Combustion behavior in air of single particles from three different coal ranks and from sugarcane bagassse”. Combust and Flame. 2011, 158: 3, pp.452-465.

[8] M. J. G Alonso, A. G. Boreggo, D. Alvarez, and R. Menéndez, “Pyrolysis behaviour of pulverized coals at different temperatures”. Fuel. 1999, 78: pp.1501-1513.

[9] W. C. Park, A. Atreya, and H. R. Baum, “Experimental and theoretical investigation of heat and mass transfer process during wood pyrolysis”. Combust and Flame. 2010, 157: pp.481-494.

[10] N. Schaffel, M. Mancini, A. Szlek, and R. Weber, “Mathematical modeling of mild combustion of pulverized coal”. Combust and Flame. 2009, 156: pp.1771-1784.

[11] H. Stadler, D. Tobrin, M. Forster, and R. Kneer, “On the influence of the char gasification reactions on NO formation in flamless coal combustion”. Combust and Flame. 2009, 156: pp.1755-1763.

[12] C. F. M. Coimbra, J. L. T. Azevedo, and M. G. Carvalho, “3-D numerical model for predicting NO_x emissions from an industerial pulverized coal combustor”. Fuel. 1994, 73: pp.1128-1134.

[13] D. F. Fletcher, B. S. Haynes, F. C. Christo, and S. D. Joseph, “A CFD based combustion model of an entrained flow biomass gasifier”. Applied Mathematical Modelling. 2000, 24: pp.165-182.

[14] A. Elfasakhany, T. Klason, and X. S. Bai, “Modelling of pulverized wood combustion using a functional group model”. Combustion Theory and Modelling. 2008, 12: 5, pp.883-904.

[15] M. Oevermann, S. Gerber, and F. Behrendt, “Numerical simulation of wood gasification in a fluidized bed reactor using Euler-Euler modelling”. Proceedings of the 4th European combustion meeting. 2009,

[16] A. C. Benim, B. Epple, and B. Krohmer, “Modelling of pulverised coal combustion by a Eulerian-Eulerian two phase flow formulation”. Progress in Computational Fluid Dynamics. 2005, 6: pp.345-361.

[17] M. Kuffa, M. C. Paul, and J. Janicka, “Combustion processes of biomass in a fluidized bed: A review and results of CFD modelling”. In: M. C. Paul(Editor). Soot: Sources, Formation and Health Effects. Nova Science, USA, 2012, pp.243-280.

[18] C. T. Bowman, “Control of combustion-generated nitrogen oxide emissions: technology driven by regulations”. Proc. Combust. Inst. 1993, 24: pp.859-878.

[19] H. Spliethoff, “Power generation from solid fuels”. Springer Heidelberg Dordrecht, London, New York, 2010.

[20] M. M. Baum, and P. J. street, “Predicting the combustion behavior of coal particles”. Combust. Sci. Tech. 1971, 3: (5), pp.231-243.

[21] M. A. Field, “Rate of combustion of size-graded fractions of char from a low rank coal between 1200K-2000K”. Combustion and Flame. 1969, 13: pp.237-252.

[22] B. F. Magnussen, and B. H. Hjertageer, “On mathematical modelling of turbulent combustion with special emphasis on soot formation and combustion”. In: 16th Symposium (International) on combustion, The combustion Institute, 1976, pp.719-729.

[23] Fluent Inc., “Fluent 6.3 user’s guide”. 2005.

[24] X. Chen, M. horio, and T. Kojima, “Numerical simulation of entrained flow coal gasifiers”. Part , Chemical Engineering Science. 2000, 55: pp.3861-3874.

[25] A. M. Mayers, “The rate of reduction of carbon dioxide by graphite”. Am. Chem. Soc. J. 1934, 56: pp.70-76.

[26] J. B. Howard, G. C. Williams, and D. H. Fine, “Fine. Kinetics of carbon monoxide oxidation in postflame gases”. Proceedings of 14th Symposium (Int.) on combustion. 1973, pp.975-986.

[27] M. Sami, K. Annamalai, and M. Wooldridge, “Co-firing of coal and biomass fuel blends”. Prog. Energy Combust. Sci. 2001, 27: pp.171-214.

[28] S. C. Hill, and L. D. Smoot, “Modelling of nitrogen oxides formation and destruction in combustion systems”. Progress in Energy and Combustion Science. 2000, 26: pp.417-458.

[29] D. W. Pershing, and J. O. L. Wendt, “Pulverized coal combustion: The influence of flame temperature and coal composition on thermal and fuel NOx”. Proc. Comb. Inst. 1977, 16: pp.389-436.

[30] W. Wang, S.D. Brown, C.J. Hindmarsh, and K.M. Thomas, “NOx release and reactivity of chars from a wide range of coals during combustion”. Fuel. 1994, 73: pp.1381-1388.

[31] P. Glarborg, A. D. Jensen, and J. E. Johnsson, “Fuel nitrogen conversion in solid fuel fired systems”. Progress in Energy and Combustion Science. 2003, 29: pp.89-113.

[32] M. Xu, J. L. T. Azevedo, and M. G. Carvalho, “Modelling of the combustion process and NOx emission in a utility boiler”. Fuel. 2000, 79: pp.1611-1619.

[33] S. V. Patankar, “Numerical heat transfer and flow flow”. Hemispher Publishing Corp., Washington, DC, 1980.

[34] J. H. Pohl, and A.F. Sarofim, “Devolatilization and oxidation of coal nitrogen”. In: 16th Symposium (International) on Combustion, Pittsburgh, 1977, pp.491-501.

[35] N. Spitz, R. Saveliev, E. Korytni, M. Perelman, E. Bar-Ziv, and B. Chudnovsky, “Prediction of performance and pollutant emission from pulverized coal utility boilers”. In: C. M. Lefebvre and N. Science(Editors). Electric Power: Generation, Transmission and Efficiency. Nova Science, Lefebvre, 2007, pp.121-170.

[36] Y. B. Yang, T. A. Naja, and B. M. Gibbs, “Hampartsoumain E Optimisation of operating parameters for NO reduction by coal reburning in a 0.2 MWt furnace”. Journal of the Institute of Energy 1997, 70: pp.9-17.

[37] S. Niksa, and S. Cho, “Conversion of fuel-nitrogen in the primary zones of pulverized coal flames”. Energy Fuels 1996, 10: pp.463-473.

[38] A. Arenillas, R. I. Backreedy, and J. M. Jones, “Modelling of NO formation in the combustion of coal blends”. Fuel. 2002, 81: (5), pp.627-636.

[39] Y. Zhang, X. Wei, L. Zhou, and H. Sheng, “Simulation of coal combustion by turbulence-chemistry char combustion model and a full two-fluid model”. Fuel. 2005, 84: pp.1798-1804.

[40] F. Boysan, W. H. Ayers, and J. Swithenbank, “A fundamental mathematical modeling approach to cyclone design”. Trans. IchemE. 1982, 60: pp.222-230.

[41] Y. Zhang, L. Zhou, X. Wei, and H. Sheng, “Numerical simulation of Nox formation in coal combustion with inlet natural gas burning”. Chinese J. Chem. Eng. 2005, 13: pp.318-323.

[42] Y. B. YANG, V. N. SHARIFI and J. SWITHENBANK, “Numerical simulation of the burning characteristics of thermally-thick biomass fuels in packed-beds” Process Safety and Environmental Protection, 2005, 83(B6): 549–558

Table 1: Kinetic constants.

Type of reaction	Reaction. no.	Kinetic parameters			*D*	*e*	Ref.
		A (units vary)	*E* (J/kmol)	*β*			
Heterogeneous	(R1)	0.002	7.9E+07	0	-	-	[23]
Heterogeneous	(R2)	0.052	1.33E+08	0	-	-	[24]
Heterogeneous	(R3)	4.4	1.62E+08	1	-	-	[25]
Heterogeneous	(R4)	1.33	1.47E+08	1	-	-	[25]
Devolatilization	(R7)	3.12E+05	7.4E+07	-	-	-	[23]
Homogeneous	(R5)	1.30E+11	1.26E+08	-	0.5	0.5	[26]
Homogeneous	(R8)	2.119E+11	2.027E+8	-	0.2	1.3	[23]

Table 2: Bituminous coal analysis data

	Proximate analysis (wt%, raw basis)				Ultimate analysis (wt%, raw basis)				
	Moisture	Volatile	Fixed carbon	Ash	C	H	O	N	S
Coal	1.57	30.46	62.87	6.67	78.9	4.9	7.6	1.3	0.6
HHV = 35084.16 KJ/Kg				LHV = 33930.32KJ/Kg					

Table 3: Reaction kinetics.

Rate of reaction	***A*(1/s)**	***E*(J/mol)**
$\boldsymbol{R_1}$	1.0×10^{10}	280451.95
$\boldsymbol{R_2}$	4.0×10^{6}	133947.2
$\boldsymbol{R_3}$	3.0×10^{12}	251151
$\boldsymbol{R_4}$	1.8×10^{8}	113017.95

Table 4: Oxygen reaction order.

Oxygen mole fraction	$\boldsymbol{a}$
$\boldsymbol{X_{o_2} \leq 4.1 \times 10^{-3}}$	1
$\boldsymbol{4.1 \times 10^{-3} \leq X_{o_2} \leq 1.11 \times 10^{-2}}$	$-3.95 - 0.9 \ln X_{o_2}$
$\boldsymbol{1.11 \times 10^{-2} \leq X_{o_2} \leq 0.03}$	$-0.35 - 0.1 \ln X_{o_2}$
$\boldsymbol{X_{o_2} \geq 0.03}$	0

Table 5: Partition of volatile nitrogen via the intermediates HCN and NH_3.

Run	**volatile nitrogen (volatile-N) partitioning**		
	% HCN	% NH_3	% NO
1	60	10	30
2	55	10	35
3	52	10	38
4	50	10	40
5	48	10	42
6	45	10	45

Table 6: Operating conditions.

Parameters	Units	Values
Coal mass flow	kg/hr	1
Wall temperature	K	1523
Volume flow rate of coal carrying air	m^3/hr	2.38
Temperature of coal carrying air	K	473
Volume flow rate of primary air	m^3/hr	4.68
Temperature of primary air	K	523
Volume flow rate of secondary air	m^3/hr	11.15
Temperature of secondary air	K	623
Mean diameter of particle	μm	16, 52, 160, 350
Mass fraction of particle diameters	%	30, 35, 25, 10

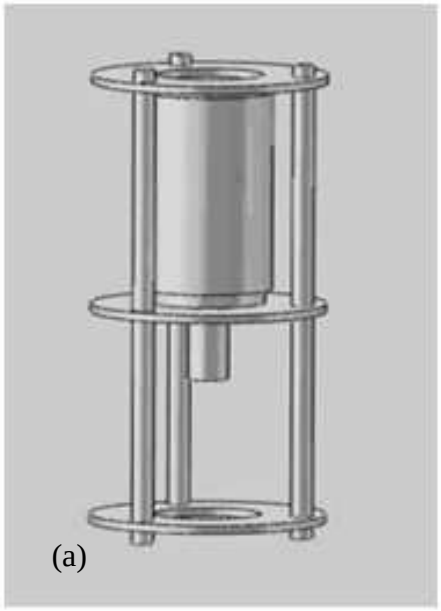

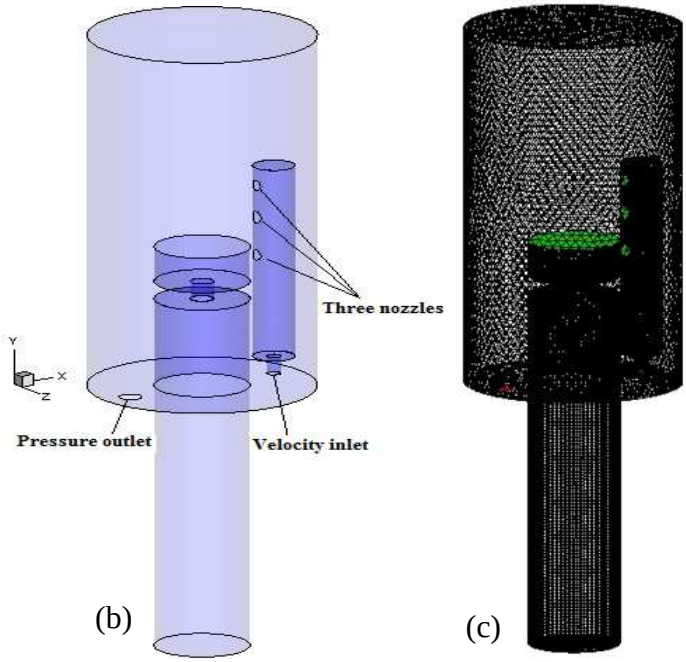

Figure 1: (a) Combustion chamber (Model 1) with holder frame, (b) computational domain and (c) grid of the domain.

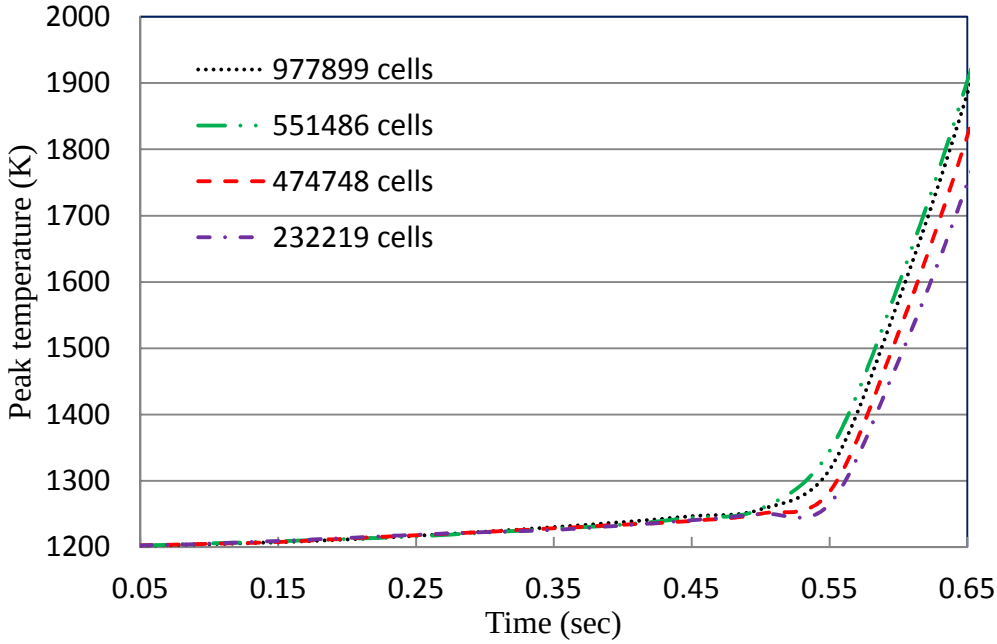

Figure 2: Maximum temperature inside the chamber (Model 1) for the particle size of 1 mm diameter.

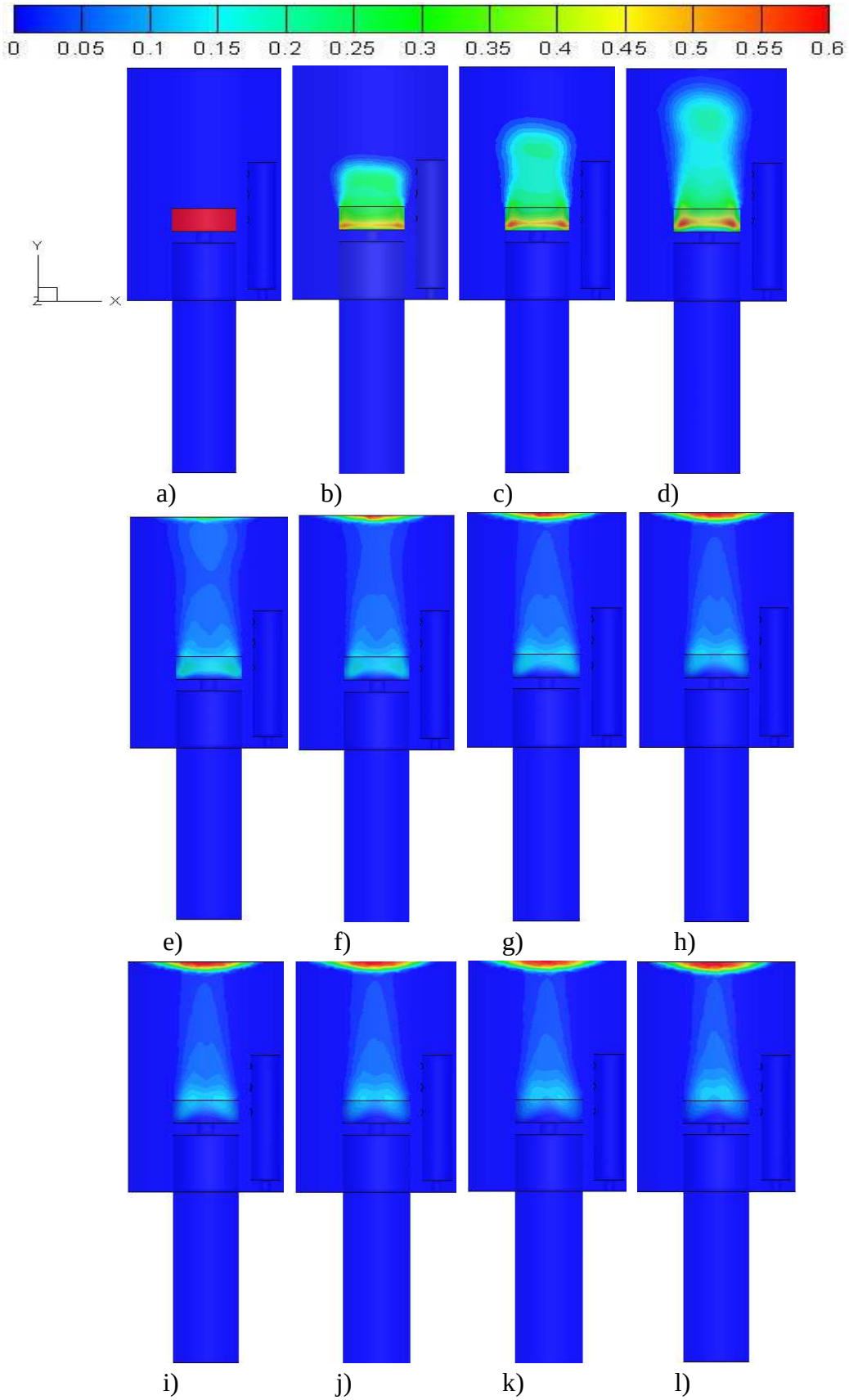

Figure 3: The variation of volume fraction of the solid phase at different simulation times (sec): (a) 0, (b) 0.05, (c) 0.1, (d) 0.15, (e) 0.2, (f) 0.25, (g) 0.30, (h) 0.35, (i) 0.40, (j) 0.45, (k) 0.50 and l) 0.55.

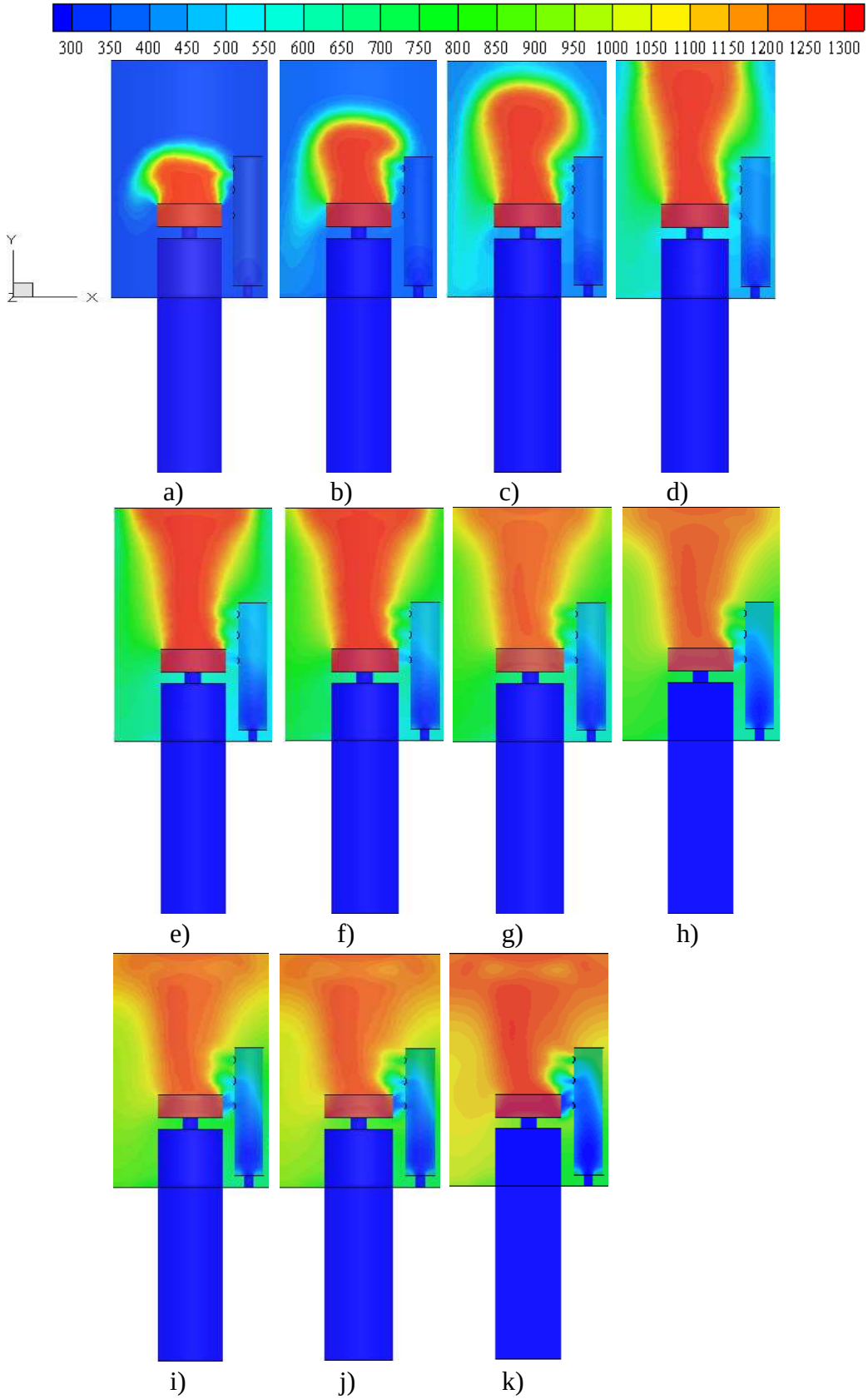

Figure 4: The variation of temperature at different timesteps for 1 mm average particle diameter showing at time (sec): (a) 0.05, (b) 0.1, (c) 0.15, (d) 0.2, (e) 0.25, (f) 0.3, (g) 0.35, (h) 0.4, (i) 0.45, (j) 0.5 and (k) 0.55.

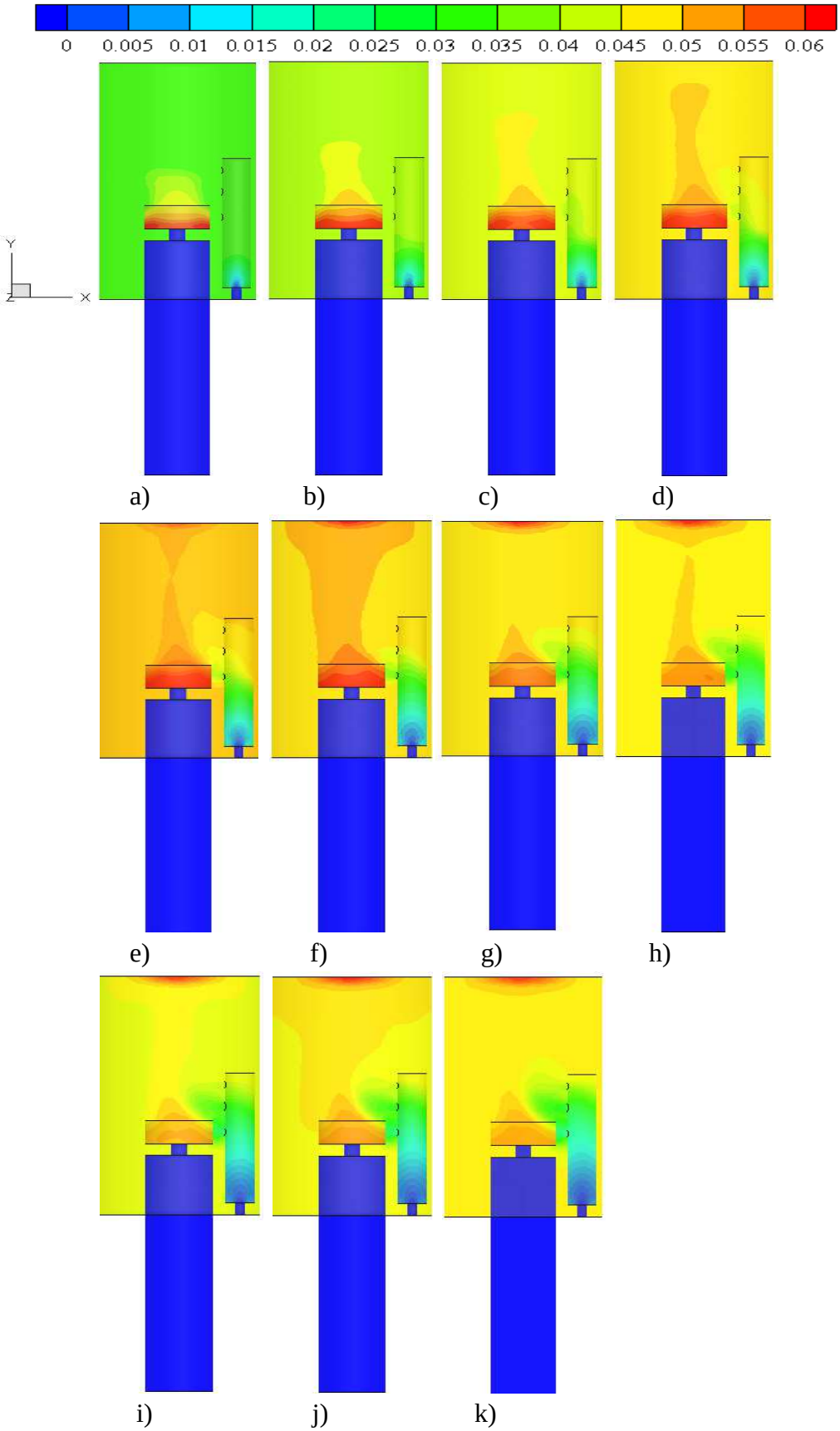

Figure 5: The mass fraction of CO_2 at different simulation times (sec): (a) 0.05, (b) 0.1, (c) 0.15, (d) 0.2, (e) 0.25, (f) 0.3, (g) 0.35, (h) 0.4, (i) 0.45, (j) 0.5 and k) 0.55.

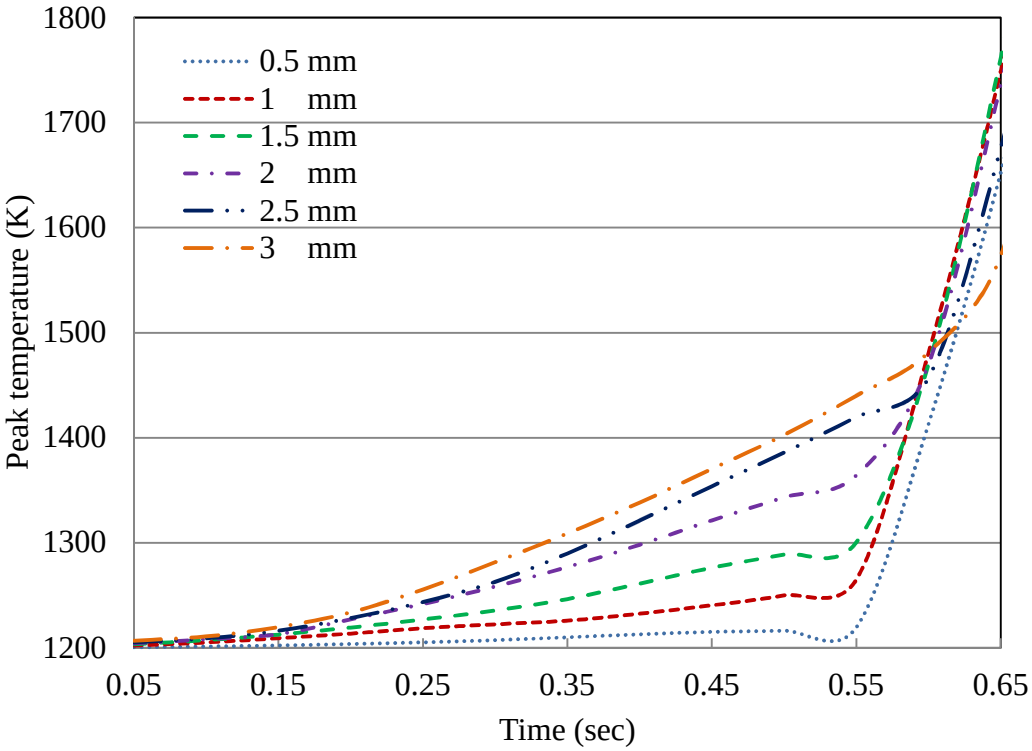

Figure 6: The peak temperature variation with time for different particle sizes.

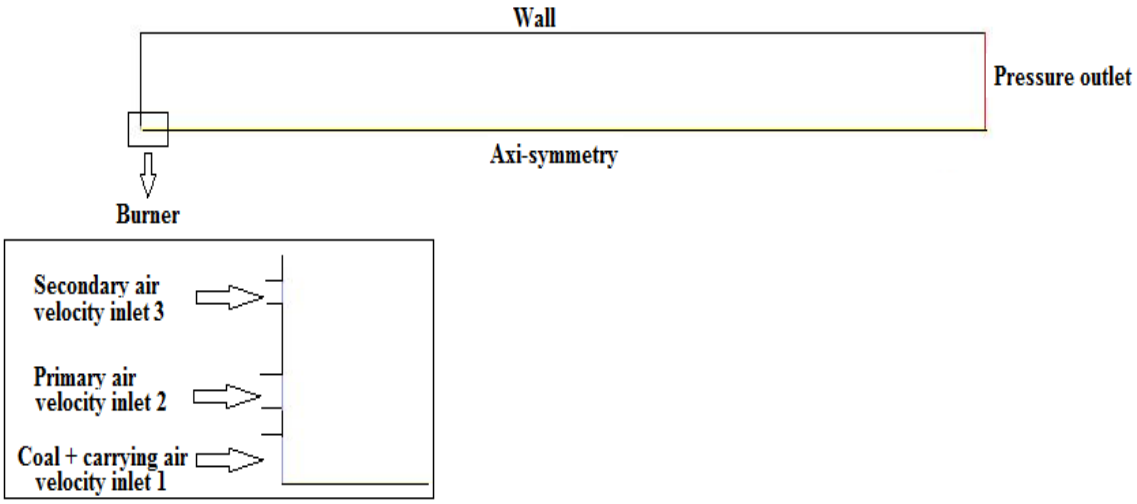

Figure 7: Geometry of the axisymmetric combustor (Model 2) Zhang et al. [39].

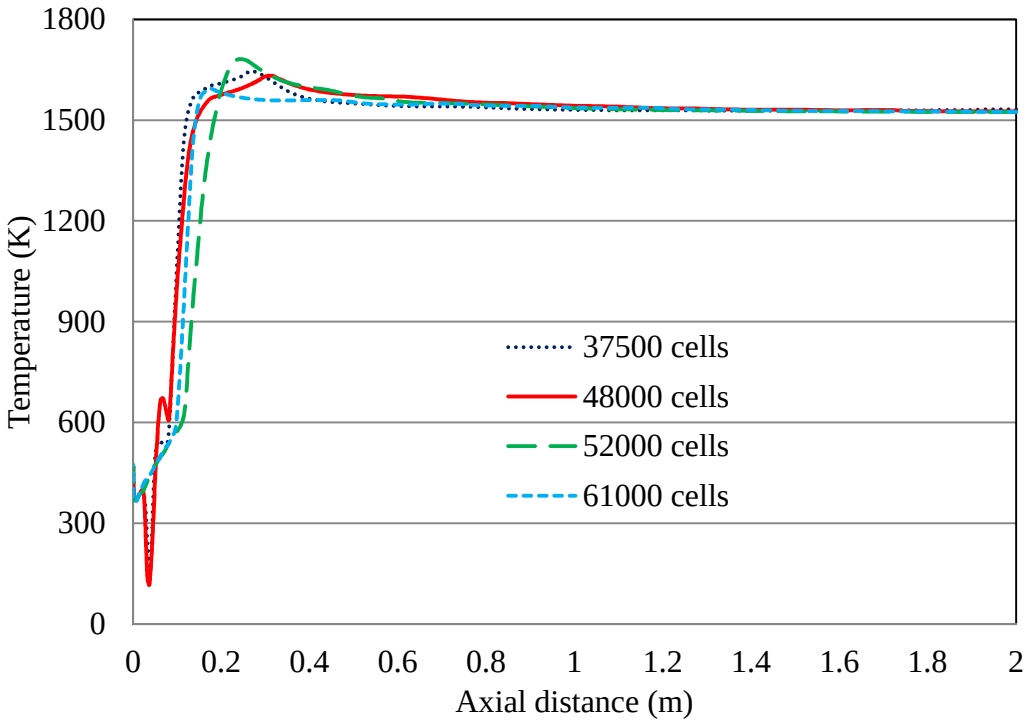

Figure 8: Maximum temperature predicted inside the reactor (Model 2) with different grids.

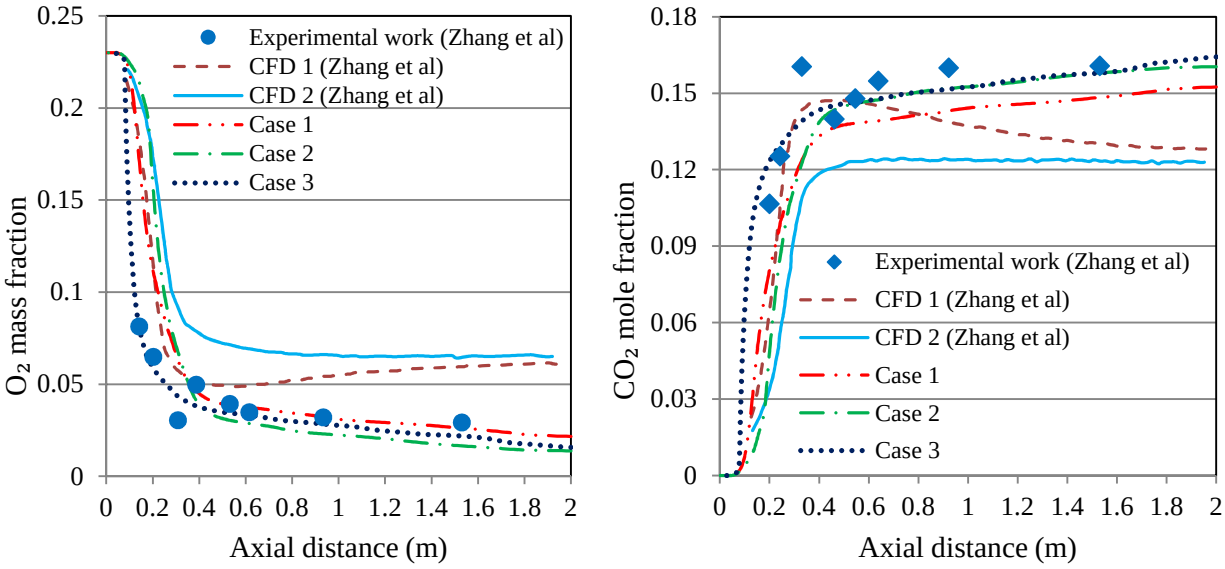

(a) (b)

Figure 9: Mass fraction of O2 along the axial distance of the reactor (a) and Mole fraction of CO2 (b) along the axial distance of the reactor.

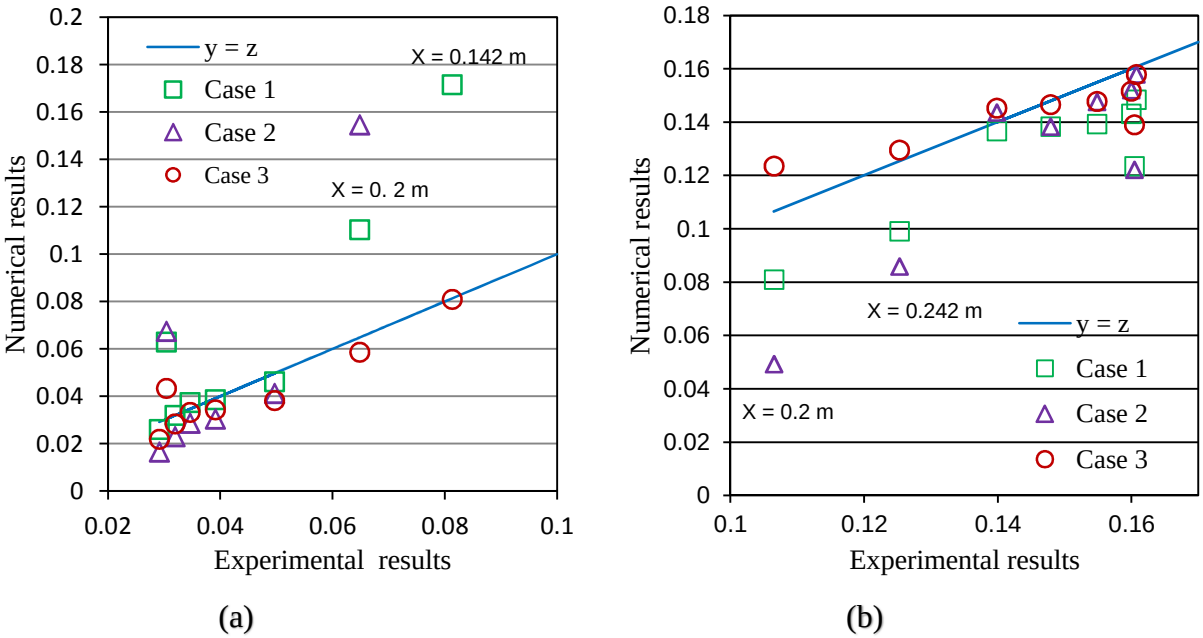

Figure 10: Comparison between the experimental and simulated data of (a) O_2 mass fraction and (b) CO_2 mole fraction. Ideal results lie on the line indicated by y = z.

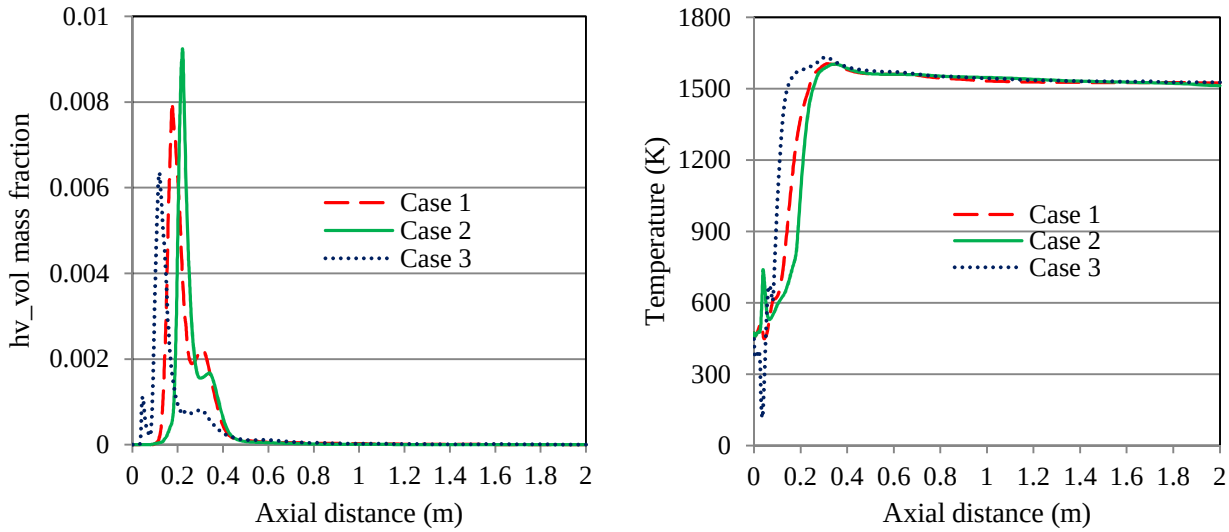

(a) (b)

Figure 11: The variation of volatile mass fraction (a) and Gas temperature (b) along the axial distance of the reactor .

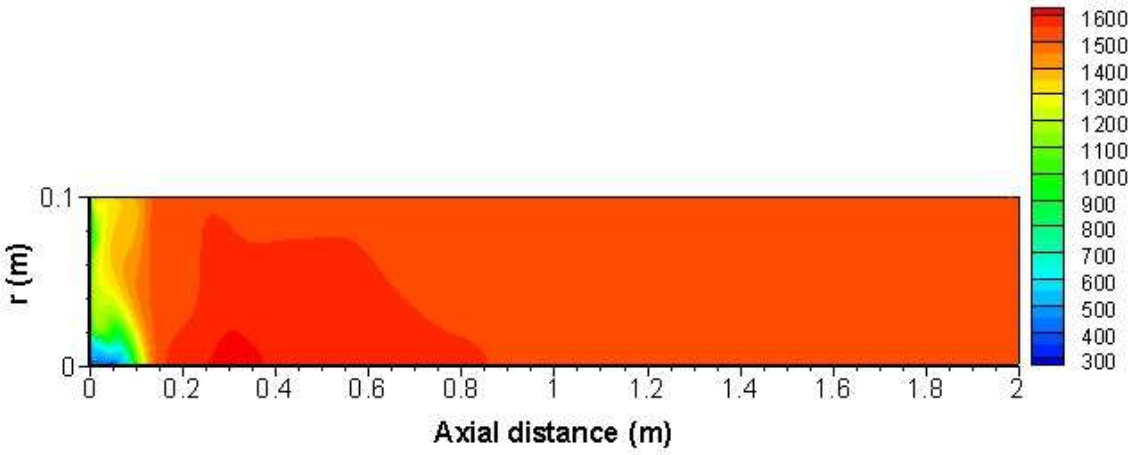

Figure 12: Gas temperature distribution of Case 3.

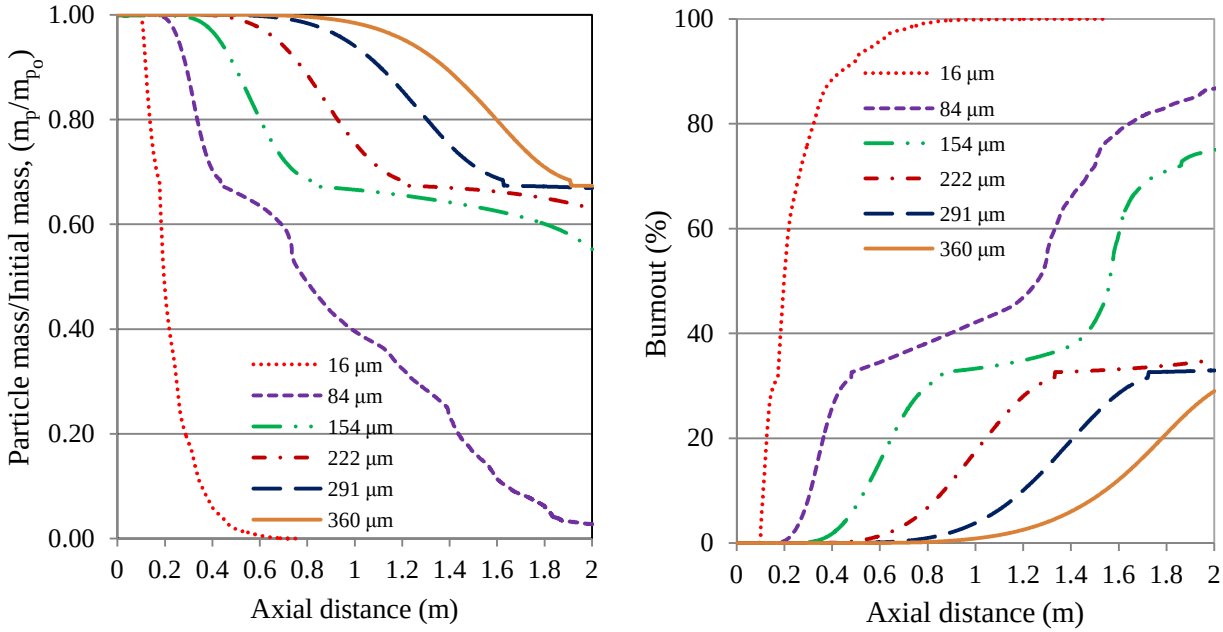

Figure 13: Mass depletion (a) and Burnout (b) of particles with different sizes for Case 3 (particle diameters in µm).

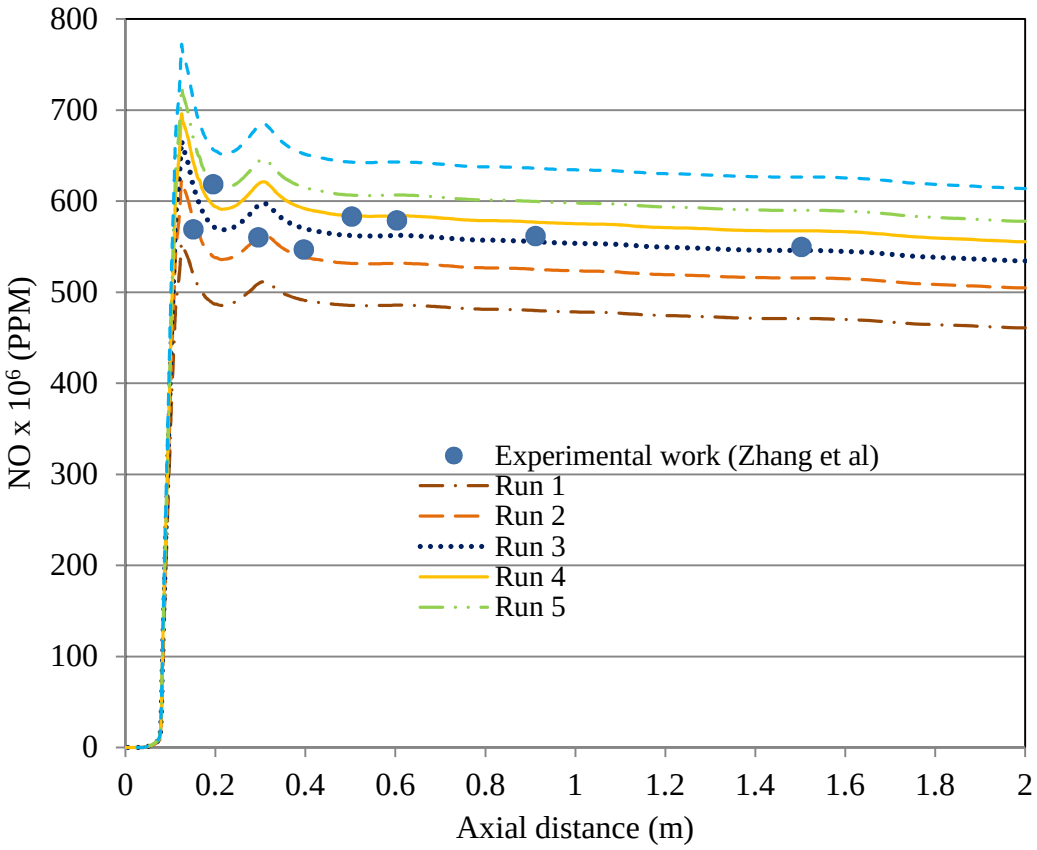

Figure 14: NO weight fraction for various runs along the axial distance of the reactor.